INTERNATIONAL JOURNAL FOR NUMERICAL METHODS IN FLUIDS
Int. J. Numer. Meth. Fluids 2004; **46**:1155–1168
Published online 29 October 2004 in Wiley InterScience (www.interscience.wiley.com). DOI: 10.1002/fld.793

Numerical analysis of deformed free surface under AC magnetic fields

Haruhiko Kohno*,† and Takahiko Tanahashi

Keio University, 3-14-1, Hiyoshi, Kohoku-ku, Yokohama 223-8522, Japan

SUMMARY

A novel numerical scheme for the analysis of large deformation of electrically conducting liquid under alternating current magnetic fields is presented. The main features are characterized by two numerical tools; the level set method to calculate deformed free surface stably and the hybrid finite element method and boundary element method to discretize the electromagnetic field efficiently. Two-dimensional numerical simulation of conducting drop deformation is carried out to demonstrate the effectiveness of the present scheme, and the oscillatory behaviour, which depends on the magnitude of surface tension and Lorentz force, is investigated. Copyright © 2004 John Wiley & Sons, Ltd.

KEY WORDS: deformed free surface; AC magnetic field; level set method; hybrid FEM–BEM

1. INTRODUCTION

Nowadays it becomes more important to introduce magnetohydrodynamics (MHD) into industry in order to achieve high purity of the products and improve productivity by controlling electrically conducting fluid flows. The idea is based on the theory that the Lorentz force, which stirs or pushes conducting liquid, is generated by the interaction between the induced current and the magnetic flux density under the alternating current (AC) magnetic field. In practice, it is carried out in some industrial applications, such as cold crucible, floating zone method and electromagnetic stirring [1]. However, in these processes, the interface becomes usually unstable due to the strong Lorentz force, and non-linear fluctuations, which give harmful effects on products, occur. Since such instability is caused by many factors, numerical simulation should be an effective tool to find out optimum conditions for these techniques.

*Correspondence to: H. Kohno, Keio University, 3-14-1, Hiyoshi, Kohoku-ku, Yokohama 223-8522, Japan.
†E-mail: kohno@tana.mech.keio.ac.jp

Contract/grant sponsor: Ministry of Education, Culture, Sports, Science and Technology

Received 16 April 2003
Revised 30 April 2004

Copyright © 2004 John Wiley & Sons, Ltd.

In the present study, we develop an effective numerical scheme that realizes coupled analysis of the flow and electromagnetic fields taking account for large deformation. Although numerous numerical studies in the area of MHD have been reported so far, the interface shapes are assumed to be constant in most cases. In the proposed scheme, a level set method [2–4] is adopted to treat the interface movement, and the governing equations of the velocity field are solved by the generalized simplified marker and cell (GSMAC) method [5, 6]. In the calculation of the electromagnetic field, the governing equations are formulated by the vector potential method and discretized by the hybrid finite element method–boundary element method (FEM–BEM). After the verification, numerical analysis of conducting drop deformation under zero gravity is carried out with the present scheme to show its effectiveness.

2. FORMULATION OF THE ELECTROMAGNETIC FIELD

First, the governing equations of the AC magnetic field are formulated by the $\mathrm{A}-\phi$ method. By employing the magnetic vector potential $\mathbf{A}$ and the electric scalar potential ϕ, the Maxwell's equations can be written in the following form:

$$\mathbf{J} = -\frac{1}{\mu_{\mathrm{m}}}\nabla^2\mathbf{A} \tag{1}$$

$$\nabla^2\mathbf{A} = \mu_{\mathrm{m}}\sigma_{\mathrm{m}}\left(\frac{\partial\mathbf{A}}{\partial t} + \nabla\phi\right) \tag{2}$$

where $\mathbf{J}, \mu_{\mathrm{m}}, \sigma_{\mathrm{m}}$ and t are the electric current density, magnetic permeability, electric conductivity and time, respectively. Here, the Coulomb gauge $\nabla\cdot\mathbf{A} = 0$ is used to lead these equations. In Equation (2), the contribution of velocity is omitted since low magnetic Reynolds number problems are solved in the present study. Consequently, the flow field has no influence on the electromagnetic field, whereas the electromagnetic field gives the Lorentz force to the flow field.

3. FORMULATION OF THE FLOW FIELD

The velocity field is governed by the equation of continuity and the incompressible Navier–Stokes equation, which are, respectively, written as follows:

$$\nabla\cdot\mathbf{v} = 0 \tag{3}$$

$$\rho\left(\frac{\partial\mathbf{v}}{\partial t} + \mathbf{v}\cdot\nabla\mathbf{v}\right) = -\nabla p + \mu\nabla^2\mathbf{v} - \sigma_{\mathrm{s}}(\nabla\cdot\mathbf{n})\mathbf{n}\delta_\varepsilon + \mathbf{J}\times\mathbf{B} \tag{4}$$

where $\mathbf{v}, \rho, p, \mu, \sigma_{\mathrm{s}}, \mathbf{n}, \delta_\varepsilon$ and $\mathbf{B}$ are the velocity, density, pressure, coefficient of viscosity, surface tension, unit normal vector pointing to the gas phase, approximate Delta function and magnetic flux density, respectively. In Equation (4), the gravity term is omitted due to zero-gravity condition. The discontinuous change of the physical properties on the free surface is

Copyright © 2004 John Wiley & Sons, Ltd.

smoothed by the approximate Heaviside function H_ε as follows:

$$\begin{cases} H_\varepsilon(F)=0 & \text{if } F<-\varepsilon \\ H_\varepsilon(F)=\dfrac{1}{2}\left\{1+\dfrac{F}{\varepsilon}+\dfrac{1}{\pi}\sin\left(\dfrac{\pi F}{\varepsilon}\right)\right\} & \text{if } |F|\leqslant\varepsilon \\ H_\varepsilon(F)=1 & \text{if } F>\varepsilon \end{cases} \tag{5}$$

where F is the level set function and ε is the smoothing bandwidth. In the present study, the liquid phase lies in $F<0$, while the gas phase does in $F>0$. The approximate Delta function is obtained by differentiating the approximate Heaviside function. The physical properties are defined in one generic equation, $q=H_\varepsilon q_{\mathrm{G}}+(1-H_\varepsilon)q_{\mathrm{L}}$ where q being the density or the coefficient of viscosity; the subscript G denotes the gas phase and L denotes the liquid phase.

The position of a free surface is captured by the level set function. The interface, $F=0$, moves according to the following advection equation:

$$\frac{\partial F}{\partial t}+\mathbf{v}\cdot\nabla F=0 \tag{6}$$

4. DISCRETIZATION OF THE ELECTROMAGNETIC FIELD

Calculation is conducted in the two-dimensional space that is composed of the FEM and BEM domains as shown in Figure 1. Equation (1) is solved in the BEM domain Ω_{B}, while Equation (2) is done in the FEM domain Ω_{A}. When the electric scalar potential is assumed to be constant in the z direction, Equations (1) and (2) are, respectively, rewritten in the following vector potential formulation:

$$J_{\mathrm{f}z}=-\frac{1}{\mu_{\mathrm{m0}}}\nabla^2 A_z \tag{7}$$

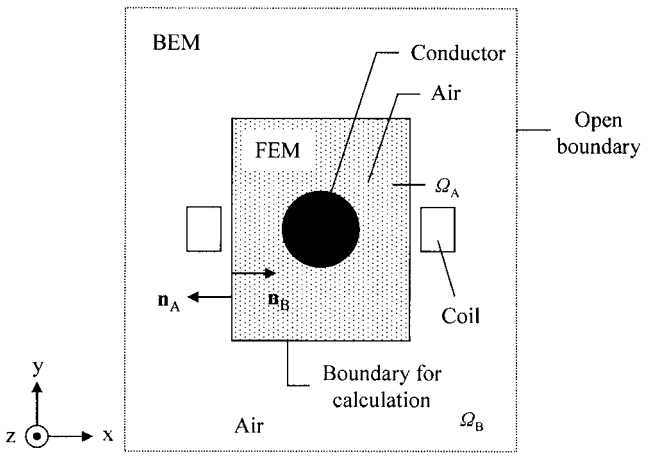

Figure 1. Calculation domains.

Copyright © 2004 John Wiley & Sons, Ltd.

$$\nabla^2 A_z = \mu_{\mathrm{m}} \sigma_{\mathrm{m}} \frac{\partial A_z}{\partial t} \tag{8}$$

where $J_{\mathrm{f}z}$ is the effective value of the alternating current flown in a coil in the z direction and $\mu_{\mathrm{m}0}$ is the magnetic permeability in a vacuum. The important point is that the physical properties in the electromagnetic field are defined in the same way as the velocity field, i.e. $q = H_\varepsilon q_{\mathrm{G}} + (1 - H_\varepsilon) q_{\mathrm{L}}$ where q being the magnetic permeability or the electric conductivity. This enables a conductive and deformed object to be solved with a level set method.

4.1. Discretization in the FEM domain

On the basis of the Galerkin method, Equation (8) is discretized as follows:

$$\begin{aligned} & j\omega \sum_{e=1}^{M} \mu_{\mathrm{m}e} \sigma_{\mathrm{m}e} \int_{\Omega_{\mathrm{A}}^e} N_\alpha N_\beta \, \mathrm{d}\Omega_{\mathrm{A}} A_{z\beta} + \sum_{e=1}^{M} \int_{\Omega_{\mathrm{A}}^e} \nabla N_\alpha \cdot \nabla N_\beta \, \mathrm{d}\Omega_{\mathrm{A}} A_{z\beta} \\ & = \sum_{e=1}^{BM} \int_{\Gamma_{\mathrm{A}}^e} N_\alpha N_\beta \, \mathrm{d}\Gamma_{\mathrm{A}} \left(\frac{\partial A_z}{\partial n} \right)_\beta \end{aligned} \tag{9}$$

where the subscripts α and β denote the local node numbers, and the variables with the subscript e are constants in the elements; M and BM are the numbers of elements in total and on the boundary, respectively; N_α and N_β are the bilinear shape functions; Γ_{A} is the boundary of Ω_{A}. Due to the assumption that the alternating current oscillates with the angular velocity ω, the magnetic vector potential can be expressed in complex number according to the Euler's formula. Thus, the time derivative $\partial/\partial t$ can be treated as $j\omega$. By using two matrices defined as

$$\begin{aligned} [N] &= j\omega \sum_{e=1}^{M} \mu_{\mathrm{m}e} \sigma_{\mathrm{m}e} \int_{\Omega_{\mathrm{A}}^e} N_\alpha N_\beta \, \mathrm{d}\Omega_{\mathrm{A}} + \sum_{e=1}^{M} \int_{\Omega_{\mathrm{A}}^e} \nabla N_\alpha \cdot \nabla N_\beta \, \mathrm{d}\Omega_{\mathrm{A}} \\ [f] &= \sum_{e=1}^{BM} \int_{\Gamma_{\mathrm{A}}^e} N_\alpha N_\beta \, \mathrm{d}\Gamma_{\mathrm{A}} \left(\frac{\partial A_z}{\partial n} \right)_\beta \end{aligned} \tag{10}$$

Equation (9) is rewritten in the following form:

$$[N][A_z] = [f] \tag{11}$$

4.2. Discretization in the BEM domain

Equation (7) is discretized by BEM as follows:

$$c_i A_{zi} + \sum_{e=1}^{BM} \int_{\Gamma_{\mathrm{B}}^e} \frac{\partial u^*}{\partial n} N_\alpha \, \mathrm{d}\Gamma_{\mathrm{B}} A_{z\alpha} - \sum_{e=1}^{BM} \int_{\Gamma_{\mathrm{B}}^e} u^* N_\alpha \, \mathrm{d}\Gamma_{\mathrm{B}} \left(\frac{\partial A_z}{\partial n} \right)_\alpha = \mu_{\mathrm{m}0} \int_{\Omega_{\mathrm{B}}} u^* J_{\mathrm{f}z} \, \mathrm{d}\Omega_{\mathrm{B}} \tag{12}$$

where the subscript i denotes the node number; c_i and u^* are the ratio of the interior angle at each node and the fundamental solution, respectively; Γ_{B} is the boundary of Ω_{B}. By using

Copyright © 2004 John Wiley & Sons, Ltd.

three matrices defined as

$$[H] = c_{ii} + \sum_{e=1}^{BM} \int_{\Gamma_B^e} \frac{\partial u^*}{\partial n} N_\alpha \, d\Gamma_B$$

$$[G] = \sum_{e=1}^{BM} \int_{\Gamma_B^e} u^* N_\alpha \, d\Gamma_B \tag{13}$$

$$[F] = \mu_{m0} \int_{\Omega_B} u^* J_{fz} \, d\Omega_B$$

Equation (12) is rewritten in the following form:

$$[H][A_z] - [G]\left[\frac{\partial A_z}{\partial n}\right] = [F] \tag{14}$$

Then the following equation can be obtained:

$$\begin{aligned} [K'][A_z] &= [M]\left[\frac{\partial A_z}{\partial n}\right] + [M][G]^{-1}[F] \\ [K'] &= [M][G]^{-1}[H] \end{aligned} \tag{15}$$

by multiplying both sides of Equation (14) by the inverse matrix of $[G]$ and the matrix $[M]$ defined as

$$[M] = \sum_{e=1}^{BM} \int_{\Gamma_B^e} N_\alpha N_\beta \, d\Gamma_B \tag{16}$$

Here, the asymmetric matrix $[K']$ is converted into a symmetric form as follows:

$$[K] = \frac{1}{2}\{[M][G]^{-1}[H] + ([M][G]^{-1}[H])^T\} \tag{17}$$

Consequently, the following equation is obtained by substituting $[K]$ for $[K']$ in Equation (15):

$$[K][A_z] = [M]\left[\frac{\partial A_z}{\partial n}\right] + [M][G]^{-1}[F] \tag{18}$$

4.3. Hybrid FEM–BEM

By adding two matrix equations formed by FEM and BEM, which are, respectively, shown in Equations (11) and (18), the following equation is led:

$$[N + K][A_z] = [M][G]^{-1}[F] \tag{19}$$

due to the combination on the boundary described as follows:

$$[f] = -[M]\left[\frac{\partial A_z}{\partial n}\right] \tag{20}$$

Copyright © 2004 John Wiley & Sons, Ltd.

In this study, $[A_z]$ is calculated by the skyline method. Then both magnetic flux density and electric current density are obtained by introducing the calculation result into the following equations:

$$\mathbf{B}_{\mathrm{e}} = \frac{\partial N_\alpha}{\partial y} A_{z\alpha}\mathbf{i} - \frac{\partial N_\alpha}{\partial x} A_{z\alpha}\mathbf{j} \tag{21}$$

$$J_{z\mathrm{e}} = -j\omega\sigma_{\mathrm{me}} N_\alpha A_{z\alpha} \tag{22}$$

where $\mathbf{i}$ and $\mathbf{j}$ are the unit vectors pointing to the x and y directions, respectively.

Therefore, the average Lorentz force $\mathbf{F}_{\mathrm{av}}$ can be calculated as follows:

$$\mathbf{F}_{\mathrm{av}} = \frac{1}{2}\,\mathrm{Re}[-J_{z\mathrm{e}} B^*_{y\mathrm{e}}\mathbf{i} + J_{z\mathrm{e}} B^*_{x\mathrm{e}}\mathbf{j}] \tag{23}$$

where the variable with the superscript $*$ denotes a conjugate complex number. By introducing the average Lorentz force into the Navier–Stokes equation, a coupled analysis of the flow and electromagnetic fields is achieved.

5. DISCRETIZATION OF THE FLOW FIELD

Equation (4) is discretized by GSMAC–FEM with the help of Equation (3) as follows:

$$\begin{aligned}\rho^n_{\mathrm{e}} \bar{M}_{\alpha\beta}\,\frac{\tilde{\mathbf{v}}_\beta - \mathbf{v}^n_\beta}{\Delta t} &= -\rho^n_{\mathrm{e}}(\mathbf{v}^n_{\mathrm{e}}\cdot\mathbf{A}_{\alpha\beta})\mathbf{v}^n_\beta - \frac{\rho^n_{\mathrm{e}}\Delta t}{2} B_{\alpha\beta}\mathbf{v}^n_\beta + \mathbf{C}_\alpha p^n_{\mathrm{e}} - \mu^n_{\mathrm{e}} D_{\alpha\beta}\mathbf{v}^n_\beta \\ &\quad -\sigma_{\mathrm{s}}\,\frac{\mathbf{C}_\gamma\cdot\mathbf{n}^n_\gamma}{\Omega^{\mathrm{e}}} M_{\alpha\beta}\mathbf{n}^n_\beta\delta^n_{\dot{c}\mathrm{e}} + M_{\alpha\beta}(\mathbf{F}_{\mathrm{av}})_\beta - \mathbf{S}_\alpha \end{aligned} \tag{24}$$

$$\phi^{(m)}_{\mathrm{pe}} = -\rho^n_{\mathrm{e}}\lambda^{-1}\,\frac{\mathbf{C}_\alpha\cdot\tilde{\mathbf{v}}^{(m)}_\alpha}{\Omega^{\mathrm{e}}} \tag{25}$$

$$p^{(m+1)}_{\mathrm{e}} = p^{(m)}_{\mathrm{e}} + \frac{\phi^{(m)}_{\mathrm{pe}}}{\Delta t} \tag{26}$$

$$\rho^n_{\mathrm{e}}\bar{M}_{\alpha\beta}\tilde{\mathbf{v}}^{(m+1)}_\beta = \rho^n_{\mathrm{e}}\bar{M}_{\alpha\beta}\tilde{\mathbf{v}}^{(m)}_\beta + \mathbf{C}_\alpha\phi^{(m)}_{\mathrm{pe}} \tag{27}$$

where the superscript n denotes the nth time step and m the iterative calculation level of the Poisson's equation; $\tilde{\mathbf{v}}$ is the intermediate value of velocity, Δt the increment of time, Ω^{e} the area of an element, λ the Laplace operator and ϕ_{p} is the modified momentum potential.

Equation (6) is discretized explicitly as follows:

$$\bar{M}_{\alpha\beta}\,\frac{F^{n+1}_\beta - F^n_\beta}{\Delta t} = -\,\mathbf{v}^{n+1}_{\mathrm{e}}\cdot\mathbf{A}_{\alpha\beta}F^n_\beta - \frac{\Delta t}{2} B'_{\alpha\beta}F^n_\beta \tag{28}$$

In Equation (28), the interface moves according to the velocity of the next time step obtained in Equation (27).

The element coefficient matrices and the boundary term are calculated as shown in Figure 2. Here, $B_{\alpha\beta}$ and $B'_{\alpha\beta}$ are the balancing tensor diffusivity (BTD), which are introduced for stabilization [7]. In Equations (24), (27) and (28), $\bar{M}_{\alpha\beta}$ is the lumped mass matrix.

Copyright © 2004 John Wiley & Sons, Ltd.

$$\mathbf{A}_{\alpha\beta} = \int_{\Omega^e} N_\alpha \nabla N_\beta d\Omega$$

$$B_{\alpha\beta} = \int_{\Omega^e} \left(\mathbf{v}_e^n \cdot \nabla N_\alpha\right)\left(\mathbf{v}_e^n \cdot \nabla N_\beta\right) d\Omega$$

$$B'_{\alpha\beta} = \int_{\Omega^e} \left(\mathbf{v}_e^{n+1} \cdot \nabla N_\alpha\right)\left(\mathbf{v}_e^{n+1} \cdot \nabla N_\beta\right) d\Omega$$

$$\mathbf{C}_\alpha = \int_{\Omega^e} \nabla N_\alpha d\Omega$$

$$D_{\alpha\beta} = \int_{\Omega^e} \left(\nabla N_\alpha\right) \cdot \left(\nabla N_\beta\right) d\Omega$$

$$M_{\alpha\beta} = \int_{\Omega^e} N_\alpha N_\beta d\Omega$$

$$\mathbf{S}_\alpha = \int_{\Gamma^e} N_\alpha \left(p^n \mathbf{n}_\Gamma^n - \mu^n \frac{\partial \mathbf{v}^n}{\partial n_\Gamma} \right)_e d\Gamma$$

Figure 2. The element coefficient matrices and the boundary term.

6. VERIFICATION OF THE NUMERICAL SCHEME

In order to prove the validity of the present scheme, the numerical results of the electromagnetic field are checked through the comparison with those obtained by Kaneko *et al.* [8] and a commercial code MAGNA. The validity of the velocity field employing a level set method is proved in the other paper [9].

Figure 3 shows the distribution of the Lorentz force obtained by hybrid FEM–BEM with the vector potential method for a 16×10 uniform mesh. The numerical result is qualitatively in good agreement with that of Kaneko *et al.*

Figure 4 shows the comparison of the magnitude of Lorentz force on the side of mercury in a container. Two types of three-dimensional numerical simulation are carried out with different discretization methods: FEM available in MAGNA and hybrid FEM–BEM with the A $-$ ϕ method. The calculation result of the two-dimensional numerical simulation corresponding to Figure 3 is also shown on the graph. In addition, the result obtained by applying the Gaussian elimination method to Equation (19), in which $[K']$ is used instead of $[K]$, is plotted to evaluate the error in symmetrization in Equation (17). The number of grids on the examined vertical plane is 160 in every case. The validity of the schemes is proved by the similarity between the profiles, although the magnitude of Lorentz force is slightly larger in the two-dimensional case compared to that in the three-dimensional case due to the simplification that the scalar potential ϕ is constant in the z direction. Since the two-dimensional calculation results show good agreement, the error due to symmetrization can be regarded as being small.

Copyright © 2004 John Wiley & Sons, Ltd.

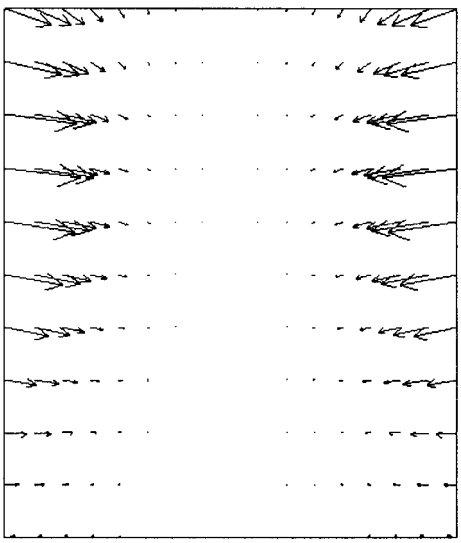

Figure 3. Distribution of the Lorentz force.

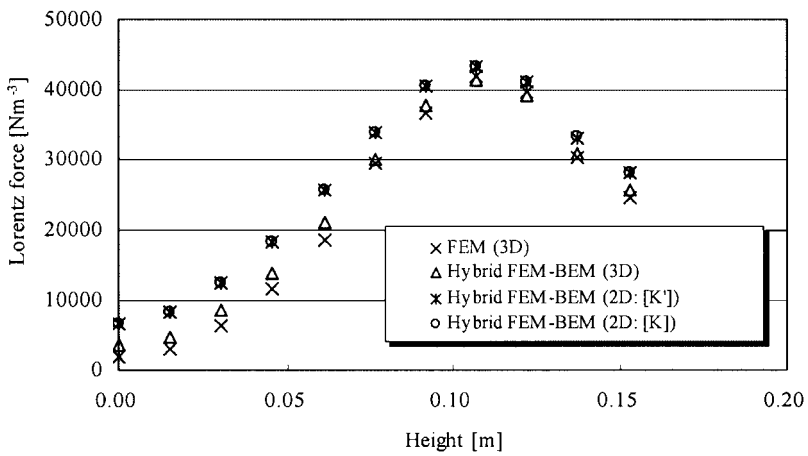

Figure 4. Comparison of the Lorentz force on the side of mercury in a container.

7. NUMERICAL ANALYSIS OF THE OSCILLATION OF A CONDUCTING DROP

7.1. Analytical model

Figure 5 shows the schematic diagram of the analytical model. A silicon drop with a radius of 0.6 cm is floated under zero gravity, and its centroid corresponds to that of the FEM domain Ω_A whose length and height are, respectively, 3.6 and 2.5 cm. Two coil sections, which are 0.5 cm square, are located on both sides of the domain, and the alternating

Copyright © 2004 John Wiley & Sons, Ltd.

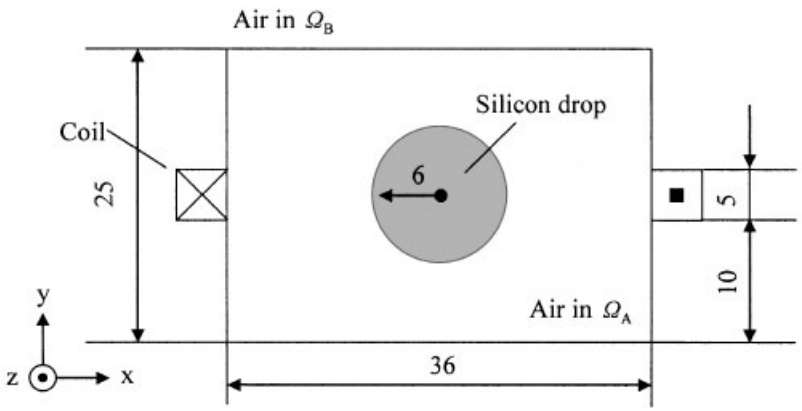

Figure 5. Schematic diagram of the analytical model.

current flows in them in the inverse directions of each other. While the frequency of the alternating current is fixed at 2.0 kHz, the following three effective values are used to vary the strength of Lorentz force: 200, 250 and 300 A. The magnitude of surface tension is also varied between 0.5 and 12 mN m^{-1} in order to investigate the relation to the oscillatory behaviour. The density, coefficient of viscosity, electric conductivity and relative permeability are 2330 kg m^{-3}, 1.00 mPa s, 1.057 MS m^{-1} and 1.0, respectively.

As the boundary condition of the velocity field, the slip condition is imposed on Γ_A. The increment of time is 0.1 ms, and the computation for the electromagnetic field is done every 10 ms. The domain is discretized into a uniform mesh of 87 (length) $\times$ 60 (height) elements. The smoothing bandwidth is set at the length of four grids in the y direction.

7.2. *Results and discussion*

Figure 6 shows the transient drop shapes and the distributions of the inside Lorentz force at $\sigma_s = 1$ mN m^{-1}, $J_{fz} = 300$ A. At first the drop deforms elliptically as shown in Figures 6(a)–(d) due to the strong Lorentz force imposed on its sides. Then the shape is restored to a circle as shown in Figures 6(e)–(h) since the restoring force at the top and the bottom of the drop becomes larger as it deforms due to the increase of curvature, while the Lorentz force on the sides becomes smaller. Therefore, the drop oscillates periodically by repeating them.

The distribution of the electric current density is shown in Figure 7 with contour lines. Here, the signs represent the direction of the physical quantity. Since a silicon drop possesses rather high electric conductivity, the induced current is generated inside the drop. The magnitude of the induced current becomes larger in the radial direction, which corresponds to the theory.

Figure 8 shows the histories of the radius length of the drop obtained by using three different effective values of the alternating current at $\sigma_s = 1$ mN m^{-1}. It is observed that all of them oscillate with a constant period. As the increase of the effective value, the amplitude becomes larger due to the strengthened Lorentz force.

Copyright © 2004 John Wiley & Sons, Ltd.

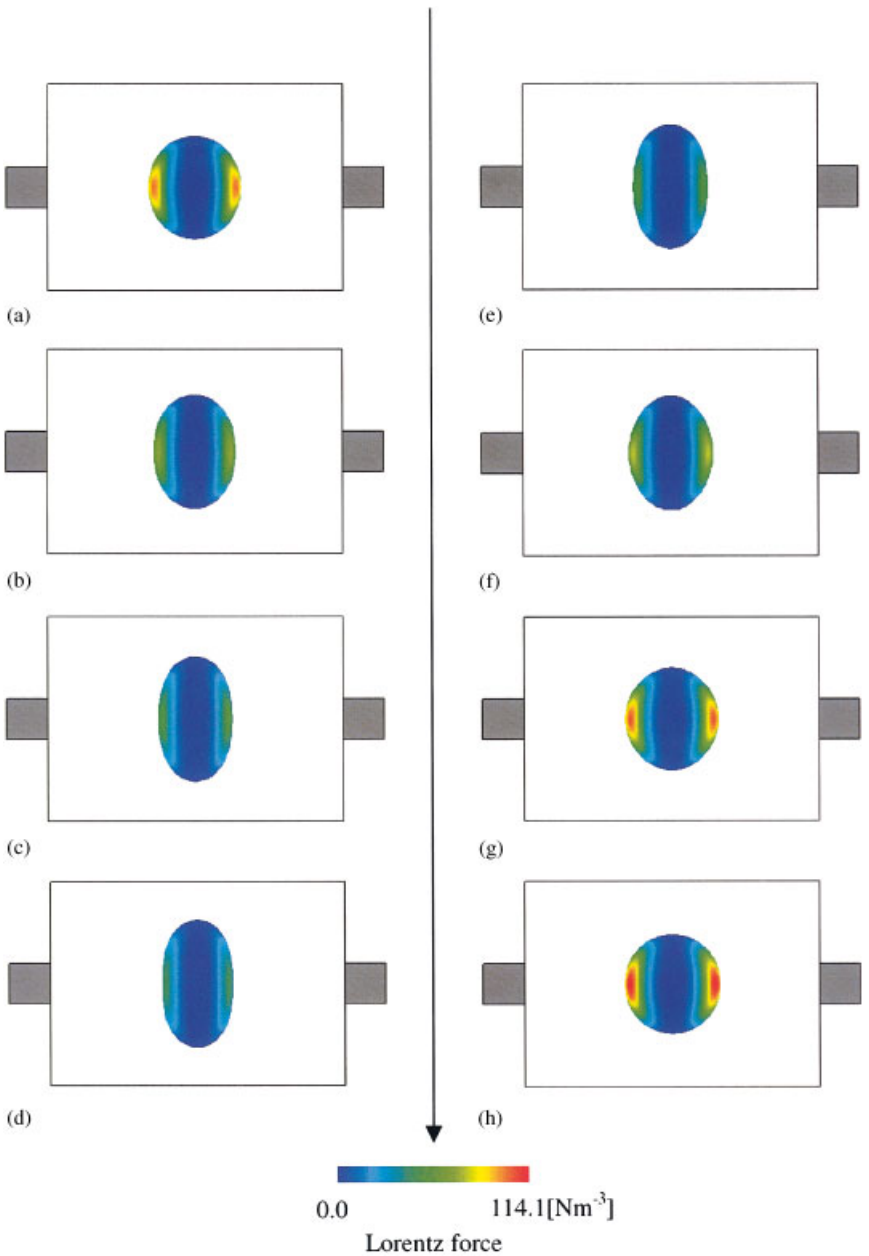

Figure 6. Transient drop shapes and the distributions of the inside Lorentz force at σ_s=1 mN m^{-1}, $J_{fz} = 300$ A: (a) 0.2 s, $F_{max} = 101.6$ Nm^{-3}; (b) 0.4 s, $F_{max} = 71.3$ Nm^{-3}; (c) 0.6 s, $F_{max} = 52.2$ Nm^{-3}; (d) 0.8 s, $F_{max} = 46.1$ Nm^{-3}; (e) 1.0 s, $F_{max} = 54.2$ Nm^{-3}; (f) 1.2 s, $F_{max} = 77.9$ Nm^{-3}; (g) 1.4 s, $F_{max} = 105.7$ Nm^{-3}; and (h) 1.6 s, $F_{max} = 114.1$ Nm^{-3}.

Copyright © 2004 John Wiley & Sons, Ltd.

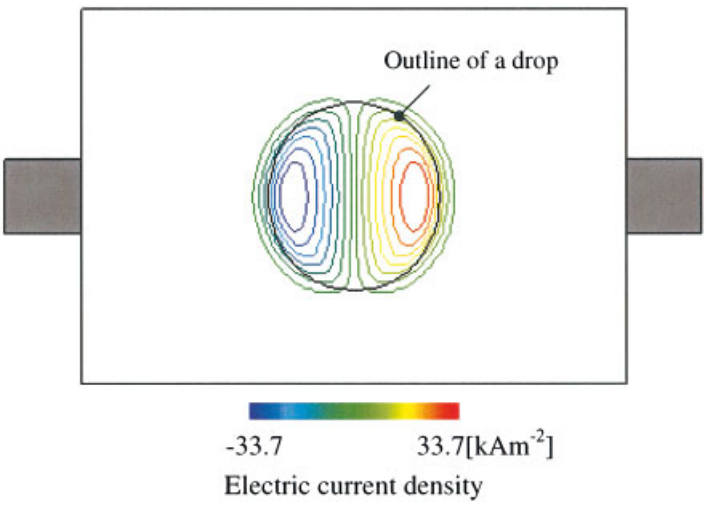

Figure 7. Distribution of the electric current density with contour lines ($\Delta J = [J_{max} - J_{min}]/15$) at $\sigma_s = 1$ mN m^{-1}, $J_{fz} = 300$ A, $t = 0.2$ s.

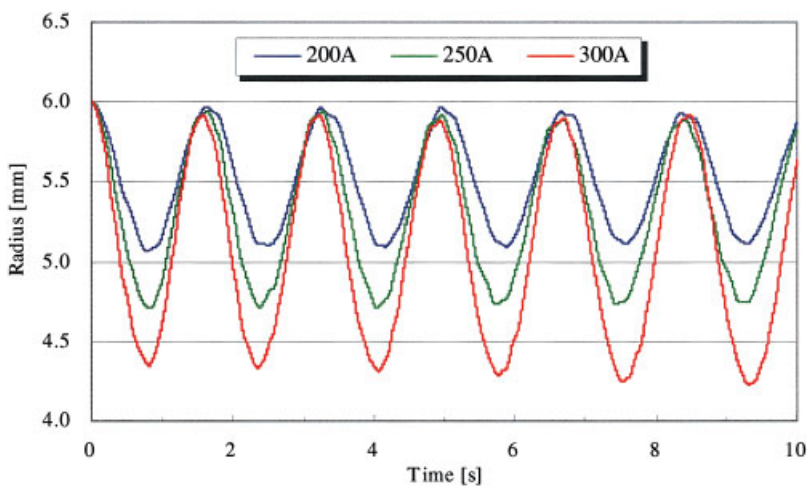

Figure 8. Histories of the radius length of the drop with three different effective values of the alternating current at $\sigma_s = 1$ mN m^{-1}.

Figure 9 shows the histories of the radius length of the drop obtained by using three different values of surface tension at $J_{fz} = 300$ A. As shown, the amplitude and the period of oscillation become, respectively, smaller and shorter as the magnitude of surface tension increases. This is caused by the fact that the Lorentz force imposed on the sides is rela-

Copyright © 2004 John Wiley & Sons, Ltd.

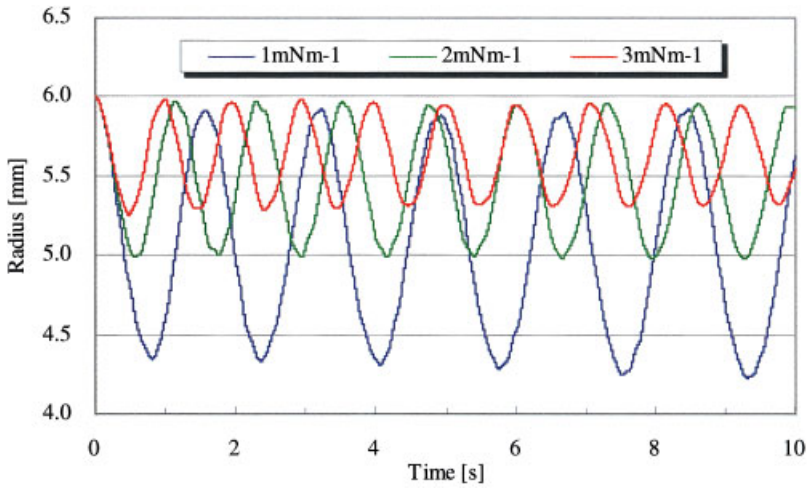

Figure 9. Histories of the radius length of the drop with three different values of surface tension at $J_{fz} = 300$ A.

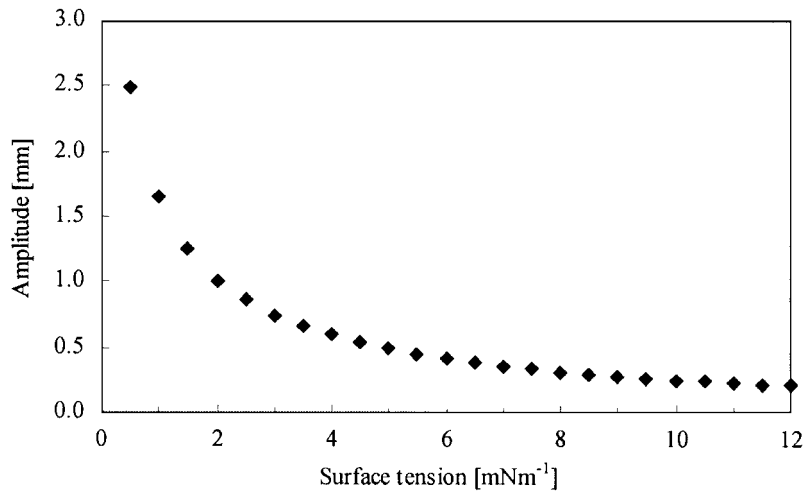

Figure 10. Relation between surface tension and amplitude of the drop oscillation at $J_{fz} = 300$ A.

tively weakened due to the strengthened restoring force at the top and the bottom of the drop.

Finally, the effect of surface tension is investigated more extensively. Figures 10 and 11 show the relation between surface tension and, respectively, amplitude and period of the drop oscillation at $J_{fz} = 300$ A. If the surface tension did not exist, a drop deformed unlimitedly due to no repulsion for the Lorentz force, and both amplitude and period became infinity. On the other hand, if the surface tension grew to infinity, both amplitude and period became

Copyright © 2004 John Wiley & Sons, Ltd.

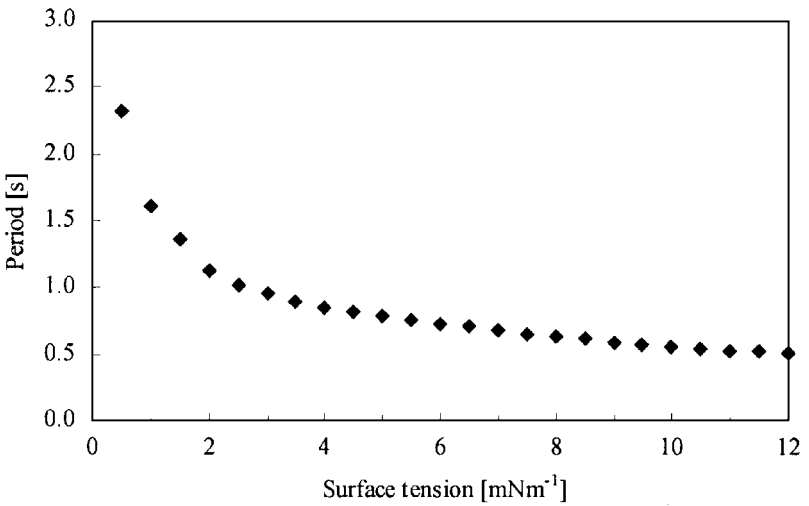

Figure 11. Relation between surface tension and period of the drop oscillation $J_{fz} = 300$ A.

infinitesimal due to infinitesimal deformation from the equilibrium state. These two results are in good agreement with the theory mentioned above.

8. CONCLUSIONS

A numerical scheme was developed to solve large deformation problems of conducting liquid under the AC magnetic field. The interface movement is solved by a level set method based on the GSMAC scheme, and the electromagnetic field is calculated with a simplified $A-\phi$ method whose formulation is discretized by hybrid FEM–BEM. To show its effectiveness, numerical analysis of conducting drop oscillation was carried out on the zero-gravity condition. As a result, it is confirmed that the oscillation of the drop is caused by the interaction between the Lorentz force and the restoring force, and its amplitude and frequency depend on the magnitude of these forces.

ACKNOWLEDGEMENTS

The authors are grateful for the support from Ministry of Education, Culture, Sports, Science and Technology under Grant-in-Aid for Scientific Research and Grant-in-Aid for JSPS Fellows.

REFERENCES

1. Davidson PA. *An Introduction to Magnetohydrodynamics* (1st edn). Cambridge University Press: Cambridge, 2001; 387–404.
2. Sussman M, Smereka P, Osher S. A level set approach for computing solutions to incompressible two-phase flow. *Journal of Computational Physics* 1994; **114**:146–159.
3. Chang YC, Hou TY, Merriman B, Osher S. A level set formulation of Eulerian interface capturing methods for incompressible fluid flows. *Journal of Computational Physics* 1996; **124**:449–464.

Copyright © 2004 John Wiley & Sons, Ltd.

4. Himeno T, Watanabe T, Konno A. Numerical analysis for propellant management in liquid rocket tank. *AIAA* 2001; **01**:3822.
5. Tanahashi T, Okanaga H, Saito T. GSMAC finite element method for unsteady incompressible Navier–Stokes equations at high Reynolds numbers. *International Journal for Numerical Methods in Fluids* 1990; **11**:479–499.
6. Tanahashi T, Oki Y, Henjes K. An application of GSMAC-FEM to electrically conducting fluid flows driven by Lorentz force. *International Journal of Computational Fluid Dynamics* 1993; **1**:233–248.
7. Dukowicz JK, Ramshaw JD. Tensor viscosity method for convection in numerical fluid dynamics. *Journal of Computational Physics* 1979; **32**:71–79.
8. Kaneko K, Tsunenari K, Sakane J, Tho T, Takeuchi E. MHD analysis on molten metal in AC magnetic field. *Proceedings of the 28th National Heat Transfer Symposium*, Japan, 1991; 634–636 (in Japanese).
9. Kohno H, Tanahashi T. Numerical analysis of moving interfaces using a level set method coupled with adaptive mesh refinement. *International Journal for Numerical Methods in Fluids* 2004; **45**:921–944.

Copyright © 2004 John Wiley & Sons, Ltd.